An Analysis of a New Approximate Model for Two-Dimensional Water Waves with Constant Vorticity

Christian Cederholm

Master's thesis
2026:E1

Lund University

Faculty of Science
Centre for Mathematical Sciences
Mathematics

CENTRUM SCIENTIARUM MATHEMATICARUM

Master's Theses in Mathematical Sciences 2026:E1
ISSN 1404-6342

LUNFMA-3162-2026

Mathematics
Centre for Mathematical Sciences
Lund University
Box 118, SE-221 00 Lund, Sweden

http://www.maths.lu.se/

An analysis of a new approximate model for two-dimensional water waves with constant vorticity

Christian Cederholm

Thesis supervisor: Evgeniy Lokharu

Date: February 4, 2026

Abstract

In this thesis, we investigate the water-wave problem for two-dimensional steady waves with constant vorticity. We introduce a new approximate model that, in its simplest form, reduces to a planar dynamical system. We then analyze this system for various energy levels and vorticity constants, studying its phase portraits to determine the locations and types of solutions that arise.

In the unidirectional regime, where the flow preserves its direction, we recover classical periodic and solitary wave solutions, including both smooth profiles and extreme waves with sharp crests. Additionally, we identify new classes of waves propagating over flows that contain a critical layer. These solutions exhibit a discontinuity in the derivative of the surface profile at a point along the side of the wave. We therefore regard them as potential prototypes of overhanging waves for the full Euler equations.

Popular science description

In this thesis, we investigate how surface waves behave when the underlying water flow has a constant rotational motion, known as vorticity. To study this, we develop a new approximate mathematical model that captures the essential dynamics of such waves. In its simplest form, this model reduces the problem to a planar dynamical system, allowing us to explore the possible wave behaviors by analyzing its trajectories.

By varying the energy and the strength of the vorticity, we map out different regimes of wave motion. In situations where the flow moves consistently in one direction, the model predicts familiar wave patterns, such as periodic waves and solitary waves. These include both smooth profiles and extreme waves with sharply pointed crests, which are known to occur in strongly nonlinear water-wave systems.

The model also reveals a new class of waves that arise when the flow contains a critical layer—a region where the horizontal velocity within the fluid matches the wave's speed. In this case, the wave surface develops a discontinuity in its slope at a specific point on the profile. These features suggest that such solutions may serve as simplified prototypes of overhanging waves, complex structures predicted by the full Euler equations but difficult to analyze directly.

Overall, the work demonstrates that our new approximate model provides a reasonable approximation to the water wave problem with vorticity, capturing the most important features at the nonlinear level.

Acknowledgements

I am deeply grateful to my supervisor, Evgeniy Lokharu, whose guidance and help have been indispensable throughout this thesis. I also extend my thanks to my family for their unwavering support.

Contents

Chapter 1

Introduction

1.1 Euler equations in 3D

We consider the motion of an ideal fluid of constant density. The fluid occupies an infinite in the horizontal directions space region with a flat bottom $y = 0$ and is separated from the air by an interface $y = \eta(x, z, t)$; see Figure 1.1. Its motion can be described by an evolution of the velocity field $\bar{u}(x, y, z, t)$, a vector assigned to every point in the fluid at every moment of time.

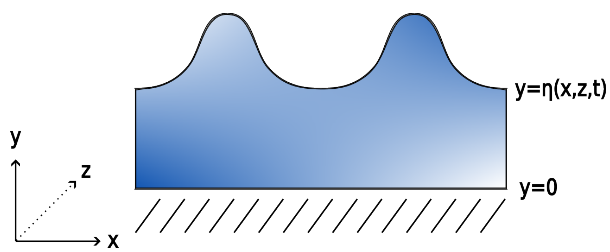

Figure 1.1: Fluid domain.

The aim of this section is to introduce mathematical equations, namely Euler equations, modeling the motion of the fluid.

We start by imagining that we have a volume of water V with constant density ρ and which is bounded inside a C^1-surface S. Then the rate at which water flows out of V through the surface is

$$\int_S \rho\bar{u} \cdot n dS,$$

where $\bar{u} = (u_1, u_2, u_3)$ is the velocity of the fluid at a point in the water and n is the normal outward unit on S (see [2] for more details); Since ρ is constant we get

$$-\int_{\partial V} \frac{d\rho}{dn} dS = -\int_{\partial V} \nabla\rho \cdot n dS = \frac{d}{dt}\int_V \rho dx = \int_V \frac{d\rho}{dt} dx = \int_V 0 dx = 0$$

meaning the change of mass in V is zero. This gives

$$0 = -\int_S \rho \bar{u} \cdot n dS,$$

and by the divergence theorem we get

$$\int_V \nabla \cdot \bar{u} dx = 0.$$

Because this must be true for any V, we conclude

$$\nabla \cdot \bar{u} = (u_1)_x + (u_2)_y + (u_3)_z = 0 \tag{1.1.1}$$

everywhere in the fluid, which is the constraint of incompressibility.

The equation (1.1.1) of incompressibility shall be complemented by an equation balancing the forces acting on a fluid particle. This equation is given by

$$\frac{D\bar{u}}{Dt} = -\frac{1}{\rho}\nabla P + (0, 0, -g), \tag{1.1.2}$$

where P is the hydrodynamic pressure, g is the gravitational constant and $\frac{D\bar{u}}{Dt}$ is the acceleration of the fluid particle as it travels along its path.

1.1.1 Boundary conditions

The boundaries of the fluid region are the surface of the water and the rigid flat bed, as shown in Figure 1.8.

The kinematic boundary condition on the surface $y = \eta(x, z, t)$ is an equation that ensures fluid particles on the surface remain on the surface and do not jump into the air or dive back into the fluid. It is expressed as

$$u_2 = \eta_t + u_1\eta_x + u_3\eta_z \quad \text{on} \quad y = \eta(x, z, t), \tag{1.1.3}$$

and on the flat bed $y = 0$ it is

$$u_2 = 0 \quad \text{on} \quad y = 0. \tag{1.1.4}$$

If there is no time dependence, then (1.1.3) simply states that the velocity field is tangential to the surface. For a time-dependent region it means that the velocity is tangential to the boundary of a 4-dimensional domain.

If we ignore the effects of air motion and surface tension, dynamic boundary condition becomes

$$P = P_{atm} \quad \text{on} \quad y = \eta(x, z, t), \tag{1.1.5}$$

where P_{atm} is the (constant) atmospheric pressure.

Thus, the water wave problem consists of the equations

$$(1.1.6)\qquad \begin{cases} \nabla \cdot \bar{u} = (u_1)_x + (u_2)_y + (u_3)_z = 0 & \text{in } \mathcal{D} \\ \frac{D\bar{u}}{Dt} = -\frac{1}{\rho}\nabla P + (0,0,-g) & \text{in } \mathcal{D} \\ u_2 = \eta_t + u_1\eta_x + u_3\eta_z & \text{on } y = \eta(x,z,t) \\ u_2 = 0 & \text{on } y = 0. \\ P = P_{atm} & \text{on } y = \eta(x,z,t) \end{cases}$$

Here $\mathcal{D} = \{(x,y,z) \in \mathbb{R}^3 : \; 0 < y < \eta(x,z;t)\}$ stands for the time-dependent fluid region.

1.1.2 Vorticity

An important characteristic of the flow is the **vorticity**, defined as

$$(1.1.7)\qquad \omega = \nabla \times \bar{u},$$

measuring the local rotation of a fluid element as seen in Figure 1.2.

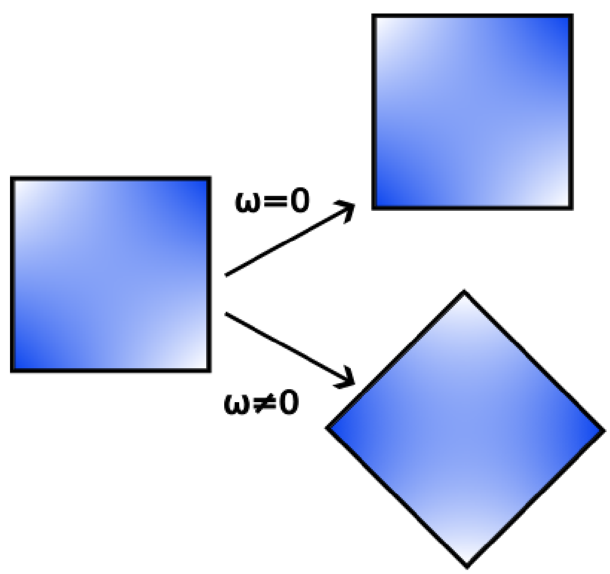

Figure 1.2: An arbitrary volume of water after small time t for $\omega = 0$ and $\omega \neq 0$.

Figure 1.2 illustrates how a fluid element depends on its vorticity. When the vorticity is zero, the element does not rotate and when the vorticity is non-zero the fluid element has a local rotation.

We can also illustrate the importance of the vorticity using laminar flows. Laminar or shear flows are solutions of the water wave problem with a flat surface for which the velocity field depends only on the depth. For such flows fluid particles move in parallel streamlines, possibly at different velocities depending on the depth. For a visual example see Figure 1.3.

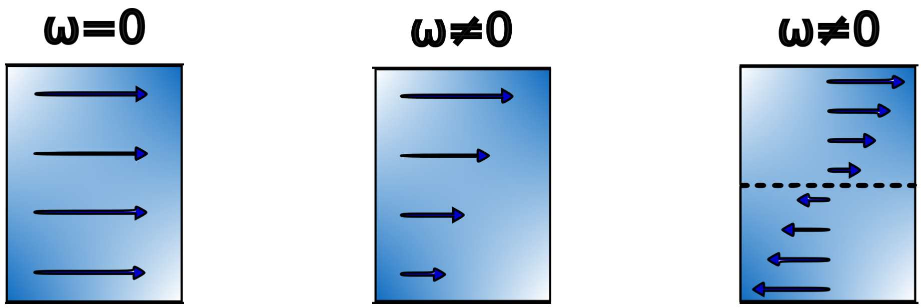

Figure 1.3: Laminar flows and shear flows.

Figure 1.3 illustrates laminar flows with and without vorticity. In Figure 1.3a, corresponding to an irrotational flow, fluid particles move with the same velocity. Figure 1.3b illustrates a shear flow, where the fluid particles have different velocities but all travel in the same direction. Figure 1.3c also shows a shear flow, but with a different property. There are two layers of the fluid, where particles travel in different directions. These layers are divided by a critical layer characterized by the zero horizontal velocity.

1.1.3 Classical solutions

Numerous solutions to the water-wave problem are known, both in the presence and absence of vorticity. One somewhat classical solution, arising as small perturbations of shear flows, are the Stokes waves. These waves are periodic and symmetric solutions, featuring precisely one crest and one trough per period P (see Figure 1.4). The first construction of irrotational Stokes waves was made by Nekrasov [6], and further details on this subject can be found in [8].

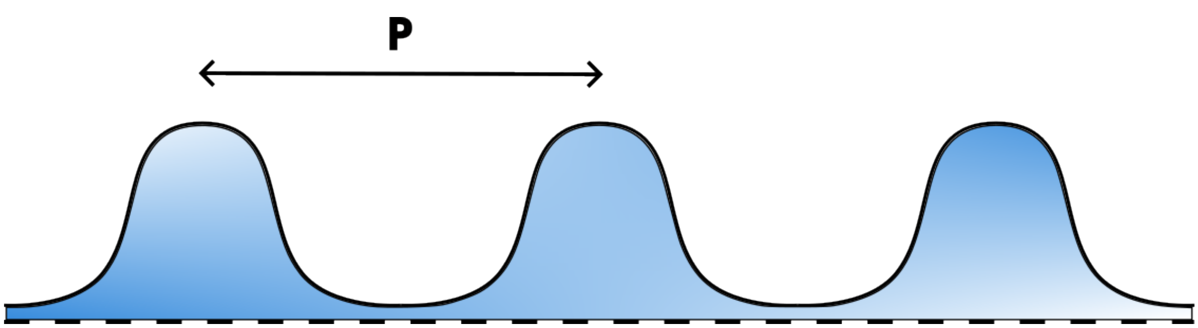

Figure 1.4: Periodic/Stokes waves.

In addition to Stokes waves, another significant class of solutions are the solitary waves. A solitary wave of height η possesses a single crest, symmetric about its peak, and decays to a uniform shear flow of depth d as $|x| \to \infty$. In a frame moving with the wave, the flow at infinity is non-zero, with velocity $u = c$, where c denotes the waves propagation speed. Conversely, in the physical frame in which the wave propagates, the fluid is still, close to infinity (see Figure

1.5). The first existence results for solitary waves were established in [5]; further discussions and explanations can be found in [3].

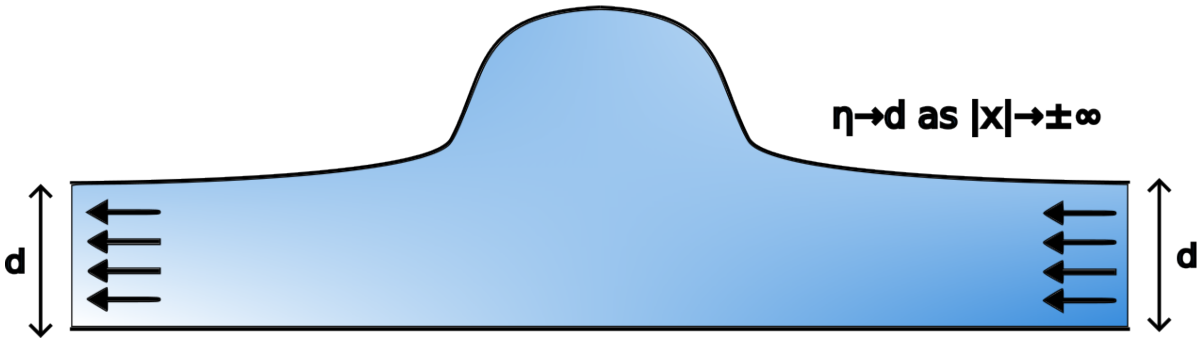

Figure 1.5: Solitary wave.

The existence of more complex solutions to the water-wave problem has remained a challenging issue for many decades. Already in [7], Stokes conjectured the existence of extreme waves, or waves of greatest height, whose surface profiles form a sharp crest with an interior angle of 120° at each peak (see Figure 1.6). It is noteworthy that both extreme solitary waves and extreme periodic waves exist. The existence of such waves was established by Amick, Fraenkel, and Toland in [1].

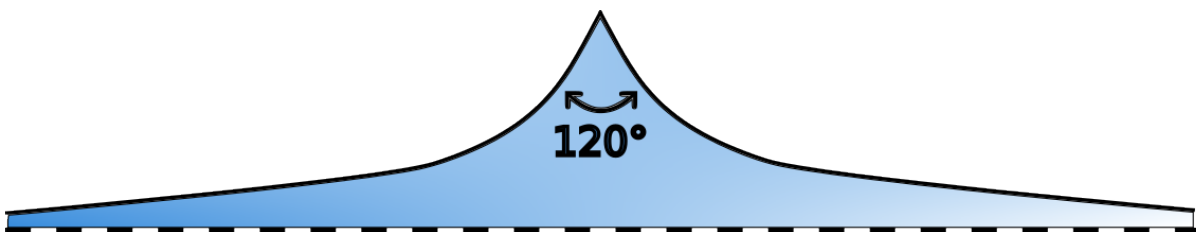

Figure 1.6: Solitary extreme wave.

In addition to extreme waves, there is considerable interest in the construction of overhanging solutions, as illustrated in Figure 1.7. It is well established that overhanging waves can occur only in rotational flows, highlighting the crucial role of vorticity.

One of the objectives of the present study is to investigate whether the new approximate model introduced in this thesis is capable of capturing such solutions.

For our model, with constant vorticity, we expect to find 4 different types of solutions: solitary waves as shown in Figure 1.5, solitary extreme waves as shown in Figure 1.6, periodic extreme waves as shown in Figure 1.4 except the waves are as in Figure 1.6 and overhanging waves as shown in Figure 1.7.

The reason we use an approximate model to study the behavior of water waves is manyfold. Firstly the real world is to complex to describe with a perfectly accurate model, any such model would be far to complicated to have any practical use. An exact solution is also far to time consuming to use and would require having complete knowledge of every variable, which is not realistically feasible. An exact solution is unnecessary as many variables have a negligible

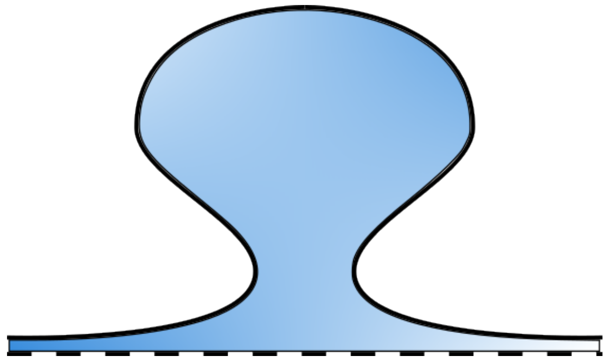

Figure 1.7: Overhanging wave.

effect on solution. For instance, the gravitational pull of Pluto does technically affect the water on earth, but in practice it can be ignored as it is to small to matter. Similarly some variables can be set to be constant, as they do not vary enough to significantly affect the result, or they do not change during the period we use our approximate model.

Our aim with studying our approximate model is to find out if it is sufficiently accurate, meaning that the results capture the most essential features of the waves.

1.2 Stream function formulation for 2D steady waves

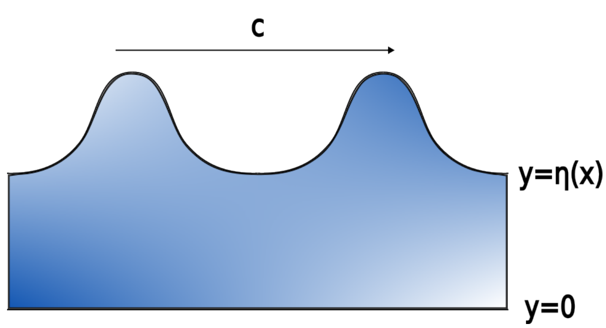

Figure 1.8: A sketch of a water wave propagating with speed c seen from the side.

In what follows we will consider two-dimensional motions, where quantities such as $\bar{u}, P, \eta$ are independent of the z variable. Furthermore, we assume a steady motion, meaning the surface profile propagates at constant speed in the positive x-direction. We choose a moving reference frame traveling at speed c such that our equations become $\eta = \eta(x - ct)$ and $P = P(x - ct)$. If we have a velocity field (u, v), and the wave has propagation speed c, then $(u - c, v) = \bar{u}$ is our relative velocity field in the moving reference frame.
In order to simplify the equations we introduce a stream function $\psi(x, y)$, defined by

$$\psi_y = u - c, \quad \psi_x = -v.$$

In the moving reference frame, a non-dimensional stream function formulation for two-dimensional steady water waves is then given below as

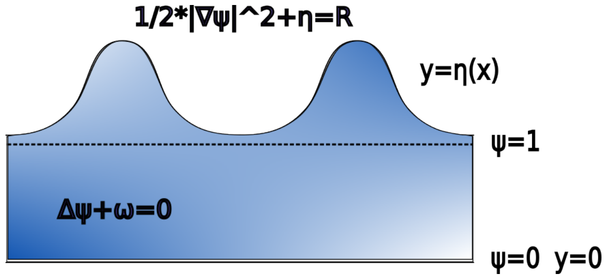

Figure 1.9: An illustration of the non-dimensional stream function formulation for two-dimensional steady water waves with constant vorticity and m scaled to unity.

$$
\begin{aligned}
\Delta\psi + \omega = \psi_{xx} + \psi_{yy} + \omega = 0 \text{ in } D_\eta;& \\
\psi = 0 \text{ on } y = 0;& \\
\psi = m \text{ on } y = \eta;& \\
\frac{1}{2}|\nabla\psi|^2 + y = r \text{ on } y = \eta.&
\end{aligned}
\tag{1.2.1}
$$

The unknown domain is defined as $D_\eta = \{(x, y) : x \in \mathbb{R}, 0 \leq y \leq \eta(x)\}$. This formulation is non-dimensional, meaning it contains no physical units and all quantities are expressed as pure numbers. Here r is the Bernoulli constant, m is the mass flux and we assume the vorticity ω to be constant; the gravitational constant is scaled to unity $g = 1$. Getting the pressure P in terms of ψ we first use the Bernoulli law

$$\frac{|\bar{u}|^2}{2} + gy + \frac{P}{\rho} = constant,$$

where $\bar{u}$ is the velocity field and g is the gravitational constant. Solving for P, setting $g = 1$ and seeing $|\bar{u}|^2 = ((u - c)^2 + v^2) = ((\psi_y)^2 + (\psi_x)^2) = |\nabla\psi|^2$ we get

$$P = \rho * constant - \frac{\rho}{2}|\nabla\psi|^2 - \rho gy.$$

The dynamic boundary condition $P = P_{atm}$ on the surface then leads to the fourth equation of (1.2.1) for $\rho = 1$ and $g = 1$.
In order to derive a new approximate model we rewrite system (1.2.1) in terms of

$$\Psi = \psi + \frac{1}{2}\omega y^2$$

as

$$
\begin{aligned}
\Psi_{xx} + \Psi_{yy} = 0 \text{ in } D_\eta;& \\
\Psi = 0 \text{ on } y = 0;& \\
\Psi = m + \frac{1}{2}\omega y^2 \text{ on } y = \eta;& \\
\frac{1}{2}\Psi_x^2 + \frac{1}{2}(\Psi_y - \omega y)^2 + y = r \text{ on } y = \eta.&
\end{aligned}
$$

Now we introduce a potential Φ from the relations

$$\Phi_x = \Psi_y, \quad \Phi_y = -\Psi_x.$$

This means that the problem in terms of Φ becomes

$$\begin{aligned} \Phi_{xx} + \Phi_{yy} &= 0 \text{ in } D_\eta; \\ \Phi_y &= 0 \text{ on } y = 0; \\ -\Phi_y + \eta_x \Phi_x &= \omega\eta\eta_x \text{ on } y = \eta; \\ \frac{1}{2}\Phi_y^2 + \frac{1}{2}(\Phi_x - \omega y)^2 + y &= r \text{ on } y = \eta. \end{aligned}$$

If Φ solves the problem above, then we can multiply the first equation by a function $P = P(y)$ to obtain an integral identity

$$\int_0^{\eta(x)} \Phi_{xx} P dy + \int_0^{\eta(x)} \Phi_{yy} P dy = 0.$$

This equality can be rewritten as

$$\left(\int_0^{\eta(x)} \Phi_x P dy\right)_x - \int_0^{\eta(x)} \Phi_y P_y dy + [\Phi_y P - \Phi_x \eta_x P]_{y=\eta(x)} = 0.$$

Now using the boundary conditions for Φ, we conclude

$$\left(\int_0^{\eta(x)} \Phi_x P dy\right)_x - \int_0^{\eta(x)} \Phi_y P_y dy - \omega\eta\eta_x P(\eta) = 0. \tag{1.2.2}$$

Thus any solution to the water wave problem has to satisfy this equality for any P. On the other-hand, if Φ solves the integral identity for all polynomials P of an arbitrary order, then one can recover both the Laplace equation and the kinematic boundary condition on the top.

Now assuming

$$\Phi = \Phi_{approximate} = \phi_0(x) + \phi_1(x)y^2 + \phi_2(x)y^4 + ... + \phi_N(x)y^{2N}.$$

solves (1.2.2) for all polynomials of order $2N$ (with only even powers) one finds a system of equations for the unknown coefficients $\phi_0, ..., \phi_N$. These equations shall be combined with the Bernoulli equation, which completes the system of approximate equations.

In this thesis we will focus on the case $N = 1$. Thus we look for an approximate solution $\Phi_{approximate} = \phi_0(x) + \phi_1(x)y^2$ that solves (1.2.2) for any $P = a_0 + a_1 y^2$. We also require that

$$\frac{1}{2}v^2 + \frac{1}{2}(u - \omega y)^2 + y = r \text{ on } y = \eta,$$

where

(1.2.3) $$u = (\Phi_{approximate})_x = \phi_0' + \phi_1'(x)y^2, \quad v = (\Phi_{approximate})_y = 2\phi_1(x)y.$$

Thus, our system of approximate equations are

(1.2.4) $$\begin{gathered} \left(\phi_0'\eta + \frac{1}{3}\phi_1'\eta^3\right)_x - \omega\eta\eta' = 0, \\ \left(\frac{1}{3}\phi_0'\eta^3 + \frac{1}{5}\phi_1'\eta^5\right)_x - \omega\eta^3\eta' = \frac{4}{3}\phi_1\eta^3, \\ \frac{1}{2}(2\phi_1\eta)^2 + \frac{1}{2}(\phi_0' + \phi_1'\eta^2 - \omega\eta)^2 + \eta = r. \end{gathered}$$

We can also assume a bit stronger equation

$$\phi_0'\eta + \frac{1}{3}\phi_1'\eta^3 = 1 + \frac{1}{2}\omega\eta^2,$$

to be true, replacing the first equation in the system above. This comes from integration of the first equation in (1.2.4), where the constant of integration is scaled to unity without loss of generality. More precisely, one shall make a change of variables to

$$\tilde{\phi}_0 = \mu_0\phi_0(\lambda x), \quad \tilde{\phi}_1 = \mu_1\phi_1(\lambda x), \quad \tilde{\eta} = \lambda\eta.$$

Then one can choose $\mu_0\lambda^2 = \lambda^4\mu_1 = C$. This choice will scale the Bernoulli in the right way without affecting the gravitational constant.

A well known variant of system (1.2.4) is the Isobe–Kakinuma model (see [4] for more details), which takes the form

(1.2.5) $$\begin{gathered} \partial_t\eta + \nabla\cdot\left(\eta\nabla\phi_0 + \frac{1}{3}\eta^3\nabla\phi_1\right) = 0, \\ \eta^2\partial_t\eta + \nabla\cdot\left(\frac{1}{3}\eta^3\nabla\phi_0 + \frac{1}{5}\eta^5\nabla\phi_1\right) = \frac{4}{3}\phi_1\eta^3, \\ \partial_t\phi_0 + \eta^2 d_t\phi_1 + \frac{1}{2}(2\phi_1\eta)^2 + \frac{1}{2}|\nabla\phi_0|^2 + \eta^2\nabla\phi_0\cdot\nabla\phi_1 + \frac{1}{2}\eta^4|\nabla\phi_1|^2 + \eta = r. \end{gathered}$$

This model is time dependent and has zero vorticity.
Now we introduce quantities

$$\alpha = 2\phi_1\eta = v|_{y=\eta}, \quad \beta = \phi_0' + \phi_1'\eta^2 - \omega\eta = u|_{y=\eta} - \omega\eta,$$

which coincide with the relative approximate velocity at the surface.

Our first goal is to obtain a first-order system for $\alpha(x)$ and $\beta(x)$ of the form

$$\begin{aligned}\alpha'(x) &= f(\alpha(x), \beta(x)),\\ \beta'(x) &= g(\alpha(x), \beta(x)),\end{aligned}$$

where f, g depend only on α, β and r (and do no depend on η). After the equations are written down we can analyze the system by plotting phase portraits for different values of r and analyzing the trajectories.

Chapter 2

Derivation of model equations

2.1 Model equations

We start with our system of approximate equations (1.2.4), which is

$$
\begin{aligned}
(\phi_0'\eta + \frac{1}{3}\phi_1'\eta^3)' - \omega\eta\eta' &= \phi_0''\eta + \phi_0'\eta' + \frac{1}{3}\phi_1''\eta^3 + \phi_1'\eta^2\eta' - \omega\eta\eta' = 0,\\
(\frac{1}{3}\phi_0'\eta^3 + \frac{1}{5}\phi_1'\eta^5)' &= \frac{1}{3}\phi_0''\eta^3 + \phi_0'\eta^2\eta' + \frac{1}{5}\phi_1''\eta^5 + \phi_1'\eta^4\eta' = \frac{4}{3}\phi_1\eta^3 + \omega\eta^3\eta',\\
\frac{1}{2}(2\phi_1\eta)^2 + \frac{1}{2}(\phi_0' + \phi_1'\eta^2 - \omega\eta)^2 + \eta &= r.
\end{aligned}
\tag{2.1.1}
$$

We can also assume

$$(\phi_0'\eta + \frac{1}{3}\phi_1'\eta^3) = 1 + \frac{1}{2}\omega\eta^2$$

to be true, replacing the first equation in system (2.1.1). Note that the first equation in (2.1.1) is still valid.
We now use the original equation 1 in (2.1.1) and solve for ϕ_0'' and ϕ_1''

$$
\begin{aligned}
\phi_0'' &= \frac{\omega\eta\eta' - \phi_0'\eta' - \frac{1}{3}\phi_1''\eta^3 - \phi_1'\eta^2\eta'}{\eta},\\
\phi_1'' &= 3\frac{\omega\eta\eta' - \phi_0''\eta - \phi_0'\eta' - \phi_1'\eta^2\eta'}{\eta^3},
\end{aligned}
\tag{2.1.2}
$$

and then use equation 2 in (2.1.1) and solve for ϕ_0'' and ϕ_1'' getting

$$
\begin{aligned}
\phi_0'' &= \frac{15\omega\eta\eta' - 3\phi_1''\eta^3 - 15\phi_1'\eta^2\eta' - 15\phi_0'\eta' + 20\phi_1\eta}{5\eta},\\
\phi_1'' &= \frac{15\omega\eta\eta' - 5\phi_0''\eta - 15\phi_1'\eta^2\eta' - 15\phi_0'\eta' + 20\phi_1\eta}{3\eta^3}.
\end{aligned}
\tag{2.1.3}
$$

Inserting ϕ_1'' from (2.1.2) into the solution for ϕ_0'' from (2.1.3) and solving for ϕ_0'' we get

$$\phi_0'' = \frac{3\phi_1'\eta^2\eta' - 10\phi_1\eta + 3\phi_0'\eta' - 3\omega\eta\eta'}{2\eta}.$$

Now we insert ϕ_0'' from (2.1.2) into the solution for ϕ_1'' from (2.1.3) and solve for ϕ_1'' to get

$$\phi_1'' = \frac{-15\phi_1'\eta^2\eta' + 30\phi_1\eta - 15\phi_0'\eta' + 15\omega\eta\eta'}{2\eta^3}.$$

This gives

$$\begin{aligned} \phi_0'' &= \frac{3\phi_1'\eta^2\eta' - 10\phi_1\eta + 3\phi_0'\eta' - 3\omega\eta\eta'}{2\eta}, \\ \phi_1'' &= \frac{-15\phi_1'\eta^2\eta' + 30\phi_1\eta - 15\phi_0'\eta' + 15\omega\eta\eta'}{2\eta^3}. \end{aligned} \tag{2.1.4}$$

Now we introduce quantities

$$\begin{aligned} \alpha &= 2\phi_1\eta, \\ \beta &= \phi_0' + \phi_1'\eta^2 - \omega\eta, \end{aligned} \tag{2.1.5}$$

this along with $(\phi_0'\eta + \frac{1}{3}\phi_1'\eta^3) = 1 + \frac{1}{2}\omega\eta^2$ gives

$$\begin{aligned} \phi_1 &= \frac{\alpha}{2\eta}, \\ \phi_0' &= \beta - \phi_1'\eta^2 + \omega\eta, \\ \phi_1' &= 3\frac{2 + \omega\eta^2 - 2\phi_0'\eta}{2\eta^3} = 3\frac{2 + \omega\eta^2 - 2\beta\eta + 2\phi_1'\eta^3 - 2\omega\eta^2}{2\eta^3} = 3\frac{2 - 2\beta\eta + 2\phi_1'\eta^3 - \omega\eta^2}{2\eta^3}, \end{aligned}$$

and solving for ϕ_1' and inserting it into the expression for ϕ_0' we get

$$\begin{aligned} \phi_1 &= \frac{\alpha}{2\eta}, \\ \phi_1' &= \frac{3\omega\eta^2 + 6\beta\eta - 6}{4\eta^3}, \\ \phi_0' &= \frac{6 + \omega\eta^2 - 2\beta\eta}{4\eta}. \end{aligned} \tag{2.1.6}$$

We now rewrite the third equation of (2.1.1) in terms of α and β from (2.1.5), then differentiate, giving us

$$\frac{d}{dx}(\frac{1}{2}\alpha^2 + \frac{1}{2}\beta^2 + \eta) = \alpha\alpha' + \beta\beta' + \eta' = \frac{d}{dx}r = 0. \tag{2.1.7}$$

From the definition of α and β we get

$$\alpha' = \frac{d}{dx}(2\phi_1\eta) = 2\phi_1'\eta + 2\phi_1\eta', \tag{2.1.8a}$$

$$\beta' = \frac{d}{dx}(\phi_0' + \phi_1'\eta^2 - \omega\eta) = \phi_0'' + 2\phi_1'\eta\eta' + \phi_1''\eta^2 - \omega\eta', \tag{2.1.8b}$$

by first inserting ϕ_1' and ϕ_1 from (2.1.6) into the expression for α' in (2.1.8) we get

$$\alpha' = \frac{3\omega\eta^2 + 2\alpha\eta\eta' + 6\beta\eta - 6}{2\eta^2},$$

and then inserting ϕ_0'' and ϕ_1'' from (2.1.4) as well as ϕ_0', ϕ_1' and ϕ_1 from (2.1.6) into the expression for β' in (2.1.8) gives us

$$\beta' = \frac{\omega\eta^2\eta' - 6\beta\eta\eta' - 6\eta' + 10\alpha\eta}{2\eta^2},$$

giving us

$$\alpha' = \frac{3\omega\eta^2 + 2\alpha\eta\eta' + 6\beta\eta - 6}{2\eta^2} := f(\alpha, \beta; \eta), \tag{2.1.9a}$$

$$\beta' = \frac{\omega\eta^2\eta' - 6\beta\eta\eta' - 6\eta' + 10\alpha\eta}{2\eta^2} := g(\alpha, \beta; \eta). \tag{2.1.9b}$$

Inserting the expressions for α' and β' from (2.1.9) into (2.1.7) and solving for η' we get

$$\eta' = -\frac{3\alpha\eta^2\omega + 16\alpha\beta\eta - 6\alpha}{\beta\eta^2\omega - 6\beta^2\eta + 2\eta\alpha^2 + 2\eta^2 - 6\beta} := h(\alpha, \beta; \eta). \tag{2.1.10}$$

Where

$$\eta = r - \frac{1}{2}\alpha^2 - \frac{1}{2}\beta^2, \tag{2.1.11}$$

which we get from equation 3 of (2.1.1), where we have inserted the values of α and β. In (2.1.9) we assume that η' is replaced by (2.1.10).
Inserting η' from (2.1.10) into (2.1.9) we get

(2.1.12)
$$\alpha' = \frac{-36\beta^3\eta^2 - 12\omega\beta^2\eta^3 + 6\eta^2(-2 + \omega\eta^2) + \beta\Big(36 - 4(6\omega + 5\alpha^2)\eta^2 + 12\eta^3 + 3\omega^2\eta^4\Big)}{2\eta^2\Big(- 6\beta^2\eta + 2\eta(\alpha^2 + \eta) + \beta(-6 + \omega\eta^2\Big)},$$

(2.1.13)
$$\beta' = \frac{\alpha\Big(- 36 + 4(6\omega + 5\alpha^2 + 9\beta^2)\eta^2 + 4(5 + 3\omega\beta)\eta^3 - 3\omega^2\eta^4\Big)}{2\eta^2\Big(- 6\beta^2\eta + 2\eta(\alpha^2 + \eta) + \beta(-6 + \omega\eta^2)\Big)}.$$

To get α' and β' independent of η we simply insert η from (2.1.11) into (2.1.12) and (2.1.13).

2.2 Linearization near equilibrium points

2.2.1 Equilibrium points

We find our equilibrium points (corresponding to laminar flows) where

$$f(\alpha, \beta; \eta) = 0, \tag{2.2.1a}$$
$$g(\alpha, \beta; \eta) = 0, \tag{2.2.1b}$$
$$\alpha = 0. \tag{2.2.1c}$$

Generally (2.2.1a) and (2.2.1b) would suffice to find equilibrium points, but solving only these two (with $\alpha \neq 0$) would give us equilibrium points corresponding to negative values for the depth, which is not physical. Thus, (2.2.1c) is added.

If $\alpha = 0$, then $\phi_1 = v = 0$, which implies

$$u = \phi_0'.$$

We then insert $\alpha = 0$ in (2.1.10) to find

$$\eta' = 0 \Rightarrow \eta = constant.$$

Inserting $\alpha = 0$, ϕ_1' and $\eta' = 0$ into (2.1.9b) and (2.1.8a) we get

$$\begin{aligned} \alpha' &= f(\alpha, \beta; \eta) = 0, \\ \beta' &= g(\alpha, \beta; \eta) = 0. \end{aligned}$$

Combining these gives us (2.2.1) and

$$\begin{aligned} \eta' &= 0, \\ \eta &= constant, \\ \phi_1 &= 0. \end{aligned}$$

Solving the equation $f(0, \beta) = 0$ for β we get

$$\beta = \frac{2 - \omega\eta^2}{2\eta} = \frac{1}{\eta} - \frac{\omega\eta}{2}. \tag{2.2.2}$$

Combining this formula with (2.1.11) we find,

$$\eta = r + \frac{\omega}{2} - \frac{1}{2}\frac{1}{\eta^2} - \frac{\omega^2\eta^2}{8},$$

which we rearrange into

$$R(\eta) := \eta + \frac{1}{2}\frac{1}{\eta^2} + \frac{\omega^2\eta^2}{8} - \frac{1}{2}\omega = r. \tag{2.2.3}$$

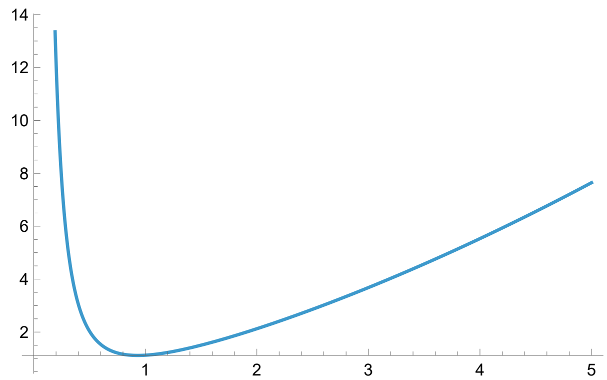

Figure 2.1: A sketch of $R(\eta)$ for $\omega = 1$.

This is the same expression as for 2d shear flow solutions for Euler equations. Thus, any solution η to this equation corresponds to an equilibrium point $(0, \beta)$ where β is given by (2.2.2).

Rearranging (2.2.3) gives

$$R(\eta) = r = \eta + \frac{1}{2}\frac{1}{\eta^2} + \frac{\omega^2\eta^2}{8} - \frac{1}{2}\omega = \eta + \frac{4 - 4\omega\eta^2 + \omega^2\eta^4}{8\eta^2} = \eta + \frac{(-2+\omega\eta^2)^2}{8\eta^2} > 0,$$

when $\eta > 0$. A sketch of the graph of $R(\eta)$ is given in Figure 2.1.

Proposition 2.2.1. *The function $R(\eta)$ is convex and so attains a global minimum R_0 for some $\eta = \eta_0 > 0$. Moreover, for any $r > R_0$ the equation* (2.2.3) *has exactly two roots $\eta_1 < \eta_2$.*

Proof. Taking the first and second derivative of the left hand side of (2.2.3) gives

$$\begin{aligned} R'(\eta) &= 1 - \frac{1}{\eta^3} + \frac{1}{4}\omega^2\eta, \\ R''(\eta) &= \frac{3}{\eta^4} + \frac{1}{4}\omega^2 > 0. \end{aligned} \tag{2.2.4}$$

□

Assuming $\eta > 0$ the first equation of (2.2.4) gives the extreme point of the equation and the second equation gives that the function is convex and thus the extreme point is a global minimum. For (2.2.3) to have solutions the value of r must be greater or equal to the value at this minimum.

2.2.2 Linearization near an equilibrium point

We linearize equations (2.1.9a) and (2.1.9b) near our equilibrium points by setting

$$\begin{aligned} \alpha &= \overline{\alpha}, \\ \beta &= \overline{\beta} + \beta_d, \\ \eta &= \overline{\eta} + d, \end{aligned} \tag{2.2.5}$$

where $\beta_d = \frac{1}{\eta} - \frac{1}{2}\omega\eta$. From (2.1.11) we get that $\overline{\eta} = -\beta_d * \overline{\beta} + O(\overline{\alpha}^2 + \overline{\beta}^2)$. We use this ansatz in (2.1.9), (2.1.10) and obtain

$$
\begin{aligned}
\overline{\alpha}' &= f_\alpha(\overline{\alpha}, \overline{\beta} + \beta_d; -\beta_d\overline{\beta} + d)|_{\overline{\alpha}=\overline{\beta}=0} \cdot \overline{\alpha} \\
&\quad + f_\beta(\overline{\alpha}, \overline{\beta} + \beta_d; -\beta_d\overline{\beta} + d)|_{\overline{\alpha}=\overline{\beta}=0} \cdot \overline{\beta} + f_\eta(\overline{\alpha}, \overline{\beta} + \beta_d; -\beta_d\overline{\beta} + d)|_{\overline{\alpha}=\overline{\beta}=0} \cdot \overline{\eta} \\
\overline{\beta}' &= g_\alpha(\overline{\alpha}, \overline{\beta} + \beta_d; -\beta_d\overline{\beta} + d)|_{\overline{\alpha}=\overline{\beta}=0} \cdot \overline{\alpha} \\
&\quad + g_\beta(\overline{\alpha}, \overline{\beta} + \beta_d; -\beta_d\overline{\beta} + d)|_{\overline{\alpha}=\overline{\beta}=0} \cdot \overline{\beta} + g_\eta(\overline{\alpha}, \overline{\beta} + \beta_d; -\beta_d\overline{\beta} + d)|_{\overline{\alpha}=\overline{\beta}=0} \cdot \overline{\eta}
\end{aligned}
\tag{2.2.6}
$$

We will reduce this system to a single equation of the form $\overline{\alpha}'' = \kappa(d,\omega)\overline{\alpha}$. Thus, computing derivatives in (2.2.6), we find

$$
\begin{aligned}
\overline{\alpha}' &= \frac{3(-4 + 4d^3 + d^4\omega^2)\overline{\beta}}{4d^4}, \\
\overline{\beta}' &= -\frac{5d^2\overline{\alpha}}{6 - d^3 - 5d^2\omega + d^4\omega^2}.
\end{aligned}
\tag{2.2.7}
$$

Taking the derivative of the first equation we get

$$
\overline{\alpha}'' = \kappa(d,\omega)\overline{\alpha}, \tag{2.2.8}
$$

where

$$
\kappa = -\frac{15(-4 + 4d^3 + d^4\omega^2)}{4d^2(6 - d^3 - 5d^2\omega + d^4\omega^2)}. \tag{2.2.9}
$$

We find bounded solutions only when $\kappa < 0$. For some choices of ω this is in fact equivalent to $\eta \in (\eta_{min}(\omega), \eta_{max}(\omega))$ which by $R(\eta)$ gives $r \in (r_{min}, r_1)$ where $r_{min} = R_0$. Here $\eta_{min}(\omega)$ and $\eta_{max}(\omega)$ are defined to be the end-points of the interval, where $\kappa < 0$. For other choices of ω the set $\kappa < 0$ might have at most two connected components; see the discussion in the next section.

2.2.3 Sign study of κ

To study the sign of κ we first divide it into its numerator and denominator

$$
\kappa = \frac{N(d,\omega)}{D(d,\omega)},
$$

where

$$
N(d,\omega) = -15(-4 + 4d^3 + d^4\omega^2).
$$

Taking the first derivative of N with respect to d we get

$$
N'(d,\omega) = -60d^2(3 + d^3\omega^2).
$$

From evaluating $N(0,\omega) = 60$, $N'(d,\omega) < 0$ for $d > 0$ and $N \to -\infty$ as $d \to +\infty$ we can see that N is positive in an interval $(0, a)$ for some positive number a and negative for $d > a$. We get a when $N(a,\omega) = 0 \Rightarrow 4a^3 + a^4\omega^2 = 4$.

If $\omega = 0$ then we have

$$D(d, 0) = 4d^2(6 - d^3),$$

which will be positive until $d > 6^{\frac{1}{3}}$ and then remain negative as $d \to +\infty$.

If $\omega \neq 0$ we have

$$D(d,\omega) = 4d^2(6 - d^3 - 5d^2\omega + d^4\omega^2),$$

which will go to infinity as $d \to +\infty$. Solving $D = 0$ for ω gives

$$\omega = \frac{5d^2 \pm \sqrt{d^4 + 4d^7}}{2d^4}.$$

We will only analyze

$$\omega = \frac{5d^2 - \sqrt{d^4 + 4d^7}}{2d^4},$$

as the other solution gives imaginary values. Taking the derivative of this equation gives us

$$\omega' = \frac{-5\sqrt{d^4 + 4d^7} + (d^2 + d^5)}{2d^4}.$$

Solving for $\omega' = 0$ gives us $(d_1 = -0.625127, d_2 = 4.61426$ and since only one of the d values is positive it is the only one we care about. Inserting d_2 into the equation for ω gives us $\omega = -0.348705$ which is the smallest ω for which D will take on negative values when $\omega \neq 0$. Thus for $\omega < -0.348705$, κ will not become positive after it becomes negative.

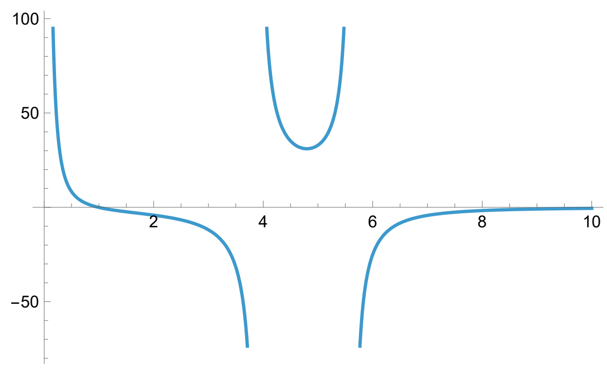

Figure 2.2: Plotting kappa as a function of η when $\omega = -0.343$.

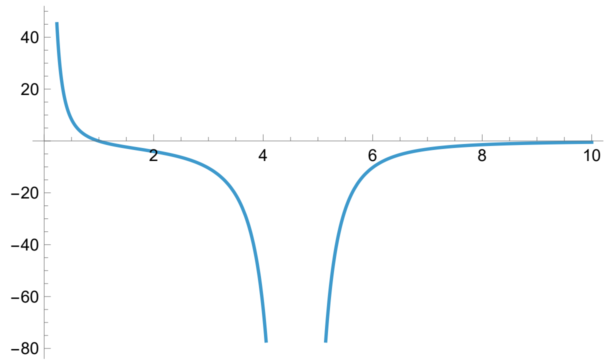

Figure 2.3: Plotting kappa as a function of η when $\omega = -0.348705$.

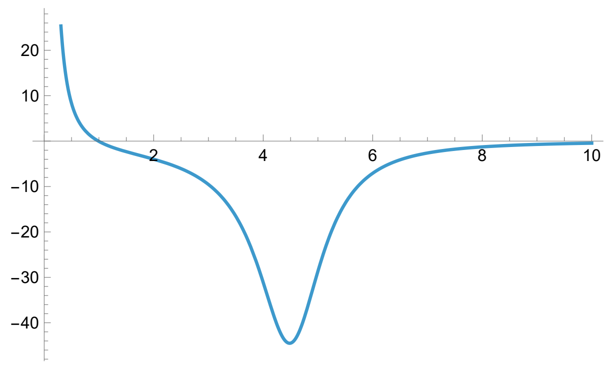

Figure 2.4: Plotting kappa as a function of η when $\omega = -0.353$.

Chapter 3

Analysis of the approximate model

3.1 Phase portrait analysis

In the previous chapter we derived analytically an approximate model for two-dimensional water waves with constant vorticity. In this section we will numerically analyze the phase portraits (which were obtained using Wolfram Mathematica) and will look for different solutions for the model. We will numerically identify the existence of various types of solutions and rigorous justifications can be made, because we deal with an explicit planar dynamical system.

For any fixed ω and r the model equations are given by

$$\alpha' = \frac{-36\beta^3\eta^2 - 12\omega\beta^2\eta^3 + 6\eta^2(-2+\omega\eta^2) + \beta\Big(36 - 4(6\omega + 5\alpha^2)\eta^2 + 12\eta^3 + 3\omega^2\eta^4\Big)}{2\eta^2\Big(-6\beta^2\eta + 2\eta(\alpha^2+\eta) + \beta(-6+\omega\eta^2)\Big)},$$

$$\beta' = \frac{\alpha\Big(-36 + 4(6\omega + 5\alpha^2 + 9\beta^2)\eta^2 + 4(5+3\omega\beta)\eta^3 - 3\omega^2\eta^4\Big)}{2\eta^2\Big(-6\beta^2\eta + 2\eta(\alpha^2+\eta) + \beta(-6+\omega\eta^2)\Big)}.$$

Here $\eta = r - \frac{1}{2}\alpha^2 - \frac{1}{2}\beta^2$.

We have already analyzed for which values of r this system possess non-trivial periodic solutions. In the irrotational case $\omega = 0$, there is an interval (r_c, r_1) for the Bernoulli constant r where one finds solutions to the linearized problem and small-amplitude periodic waves. In the next section we will explain how the structure of solutions evolves with the increase of r.

For non-zero values of $\omega > 0$ there are two intervals $(r_c(\omega), r_1(\omega))$ and $(r_2(\omega), +\infty)$ supporting small-amplitude solutions. The first interval supports unidirectional laminar flows, while the second one corresponds to flows with a surface counter current. In what follows we will analyze the structure of the solution set corresponding to these two parameter intervals.

Finally, in the last subsection we will present our findings for the remaining case of $\omega < 0$, which structure changes greatly as ω decreases.

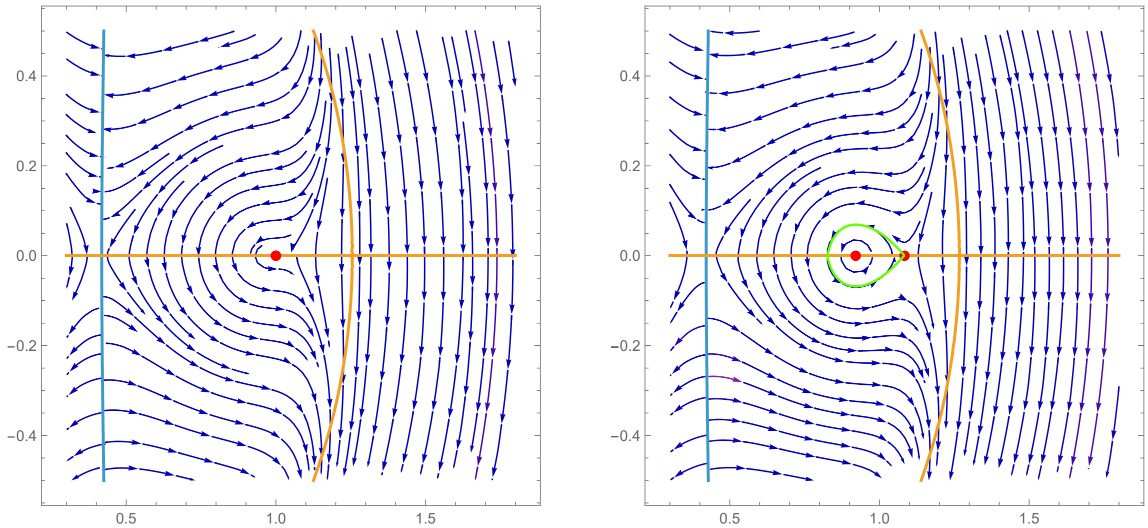

(a) Phase portrait when $\omega = 0$ and $r = 1.5$.

(b) Phase portrait when $\omega = 0$ and $r = 1.51$.

Figure 3.1

3.1.1 $\omega = 0$

We compare our approximate model in the simplest case of zero vorticity as we expect the solutions to be similar to the Euler equations. Note that for $\omega = 0$ the class of laminar flow of our approximate model is the same as for the Euler equations.

As shown in proposition 2.2.1, (2.2.3), we must have a global minimum, which we denote r_c. Thus for our system to have solutions, r must be larger than or equal to r_c. For $\omega = 0$ we have solutions in a closed interval $[r_c\,, r_1]$, and the different types of phase portraits and their corresponding solutions can be seen in Figure 3.1, 3.2, 3.3 and 3.4.

Figure 3.1a displays the phase portrait for $r = r_c$ where β is the horizontal axis and α is the vertical axis. The red dot is the equilibrium point and the light blue curve (the singularity curve) represents the set where $Den(\eta') = Den(\beta') = 0$. Here $Den(\eta')$ and $Den(\beta')$ denote the denominators of η' from (2.1.10) and β' from (2.1.13), respectively. The orange curves are the sets where the numerator of β' from (2.1.13) is zero. At $r = r_c = 1.5$, the two equilibrium points coincide, and no periodic orbits are present.

As we increase $r > r_c$ the two equilibrium points split and one finds two types of solutions. In Figure 3.1b, periodic orbits appear surrounding the left equilibrium point. These solutions converge to a limit cycle (the green curve) whose orbit passes through the second equilibrium point (note that here and elsewhere, by a limit cycle we mean an orbit given by a limit of periodic orbits; that is a homoclinic orbit can be called a limit cycle according to our terminology). This limit cycle corresponds to a solitary wave solution. Figure 3.2a illustrates the solution of Figure 3.1b. Solutions are obtained by plotting $\eta = r - \frac{1}{2}\alpha^2(x) - \frac{1}{2}\beta^2(x)$, where α and β are obtained by solving (2.2.1) numerically (using Mathematica) and β passes through some β_{guess}.

Continuing to increase r, we see a form of competition arises: the limit cycle may either hit the second equilibrium point as before or the blue singularity curve. At some point this

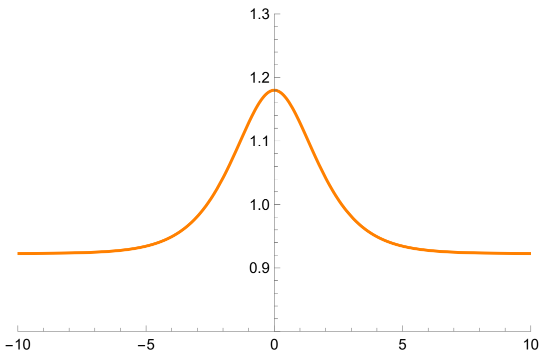

(a) A solution corresponding to the green curve in Figure 3.1b, passing through ($\beta = 0.8125773925, \alpha = 0$).

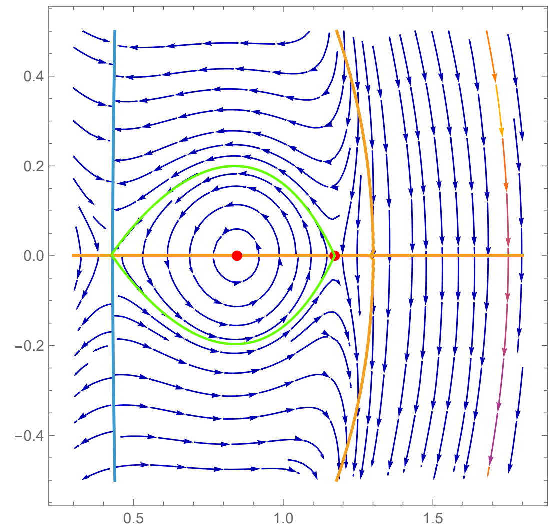

(b) Phase portrait when $\omega = 0$ and $r = 1.54$.

Figure 3.2

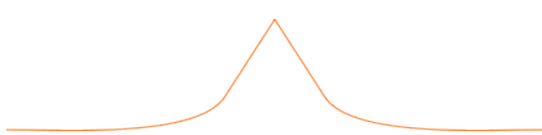

(a) A sketch of the solution corresponding to the green curve in Figure 3.2b.

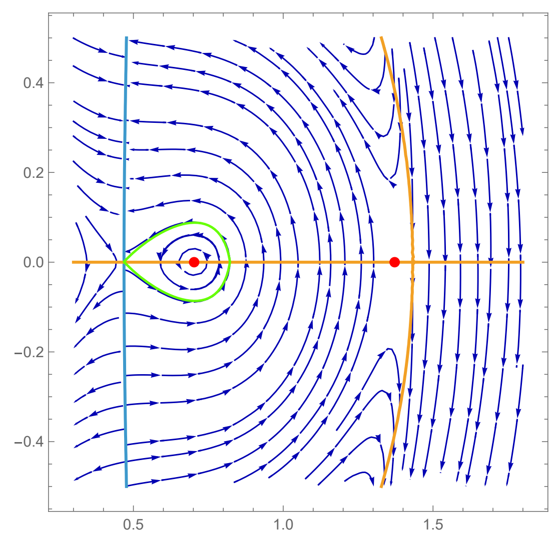

(b) Phase portrait when $\omega = 0$ and $r = 1.67$.

Figure 3.3

happens simultaneously, as illustrated in Figure 3.2b. Here the limit cycle intersects both the other equilibrium point and the singularity curve, which corresponds to an extreme solitary wave solution; see Figure 3.3a. The surface profile η is a Lipschitz function and the sharp angle at the crest is computed to be $\theta = 111.837°$, which is remarkably close to $120°$ for classical extreme waves in Euler equations. The angle is obtained using (2.1.10) (as η' is the slope of η) by setting $\tan(\theta) = \eta' = \frac{P}{Q}$ where P is the numerator of η' and Q is the denominator. η' is evaluated where the singularity curve passes through $\alpha = 0$. At this point both $P = Q = 0$ so using L'Hôpital's rule we get $\eta' = \frac{P}{Q} = \frac{P'}{Q'}$ which gives $\theta = \arctan(\frac{P'}{Q'})$.

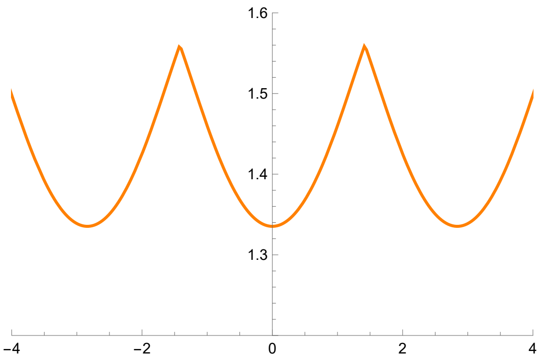

(a) A solution corresponding to the green curve in Figure 3.3b, passing through ($\beta = 0.8181503, \alpha = 0$).

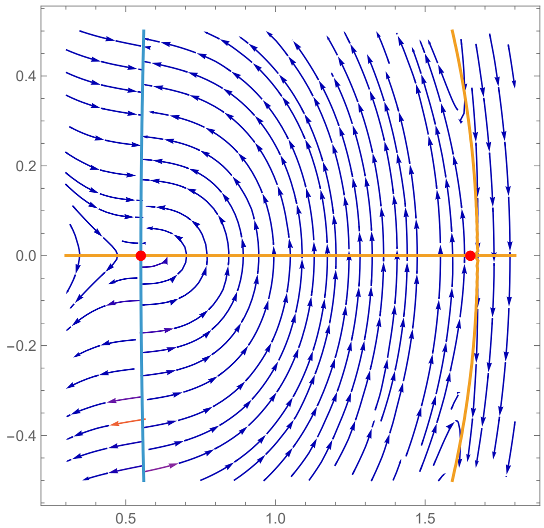

(b) Phase portrait when $\omega = 0$ and $r = 1.96855$.

Figure 3.4

This and other singular solutions we found have continuous surface profiles for which the derivative has a jump at isolated points. In this case, as can be seen from (2.1.9a)-(2.1.9b), the functions α and β are Lipschitz. Thus, the corresponding solutions shall be understood in a weak sense.

If one increases r even further, then the limit cycle will always hit the blue singularity curve first. At the same time the stable equilibrium point moves closer to the singularity curve (see Figure 3.3b). The corresponding solutions are extreme Stokes waves as can be seen in Figure 3.4a. Figure 3.4a shows the solution of Figure 3.3b and the angle is $\theta = 116.46°$ for this solution.

Once the equilibrium point crosses the blue line, it becomes unstable and no periodic solutions exist; see Figure 3.4b for $r = r_1$. For $r > r_1$ the left equilibrium point moves to the left (though it never passes zero) and the right equilibrium point moves to the right until it sits on the orange curve.

Note that all irrotational solutions presented above are unidirectional, that is $\psi_y > 0$ everywhere in the fluid. This agrees with the classical irrotational theory.

3.1.2 $\omega > 0$

Next we consider the model for $\omega > 0$, which, as we will show, differs in some ways from the irrotational setting. In particular, we find new interesting solutions.

For $\omega > 0$ we not only have a closed interval $[r_c\ , r_1]$ as previously but also a half-open interval $[r_2, \infty)$ supporting small-amplitude waves. In the following we will discuss the structure of solutions in detail.

Figure 3.5a shows the phase portrait for $r = r_c = 1.1162$. Just as in the irrotational case

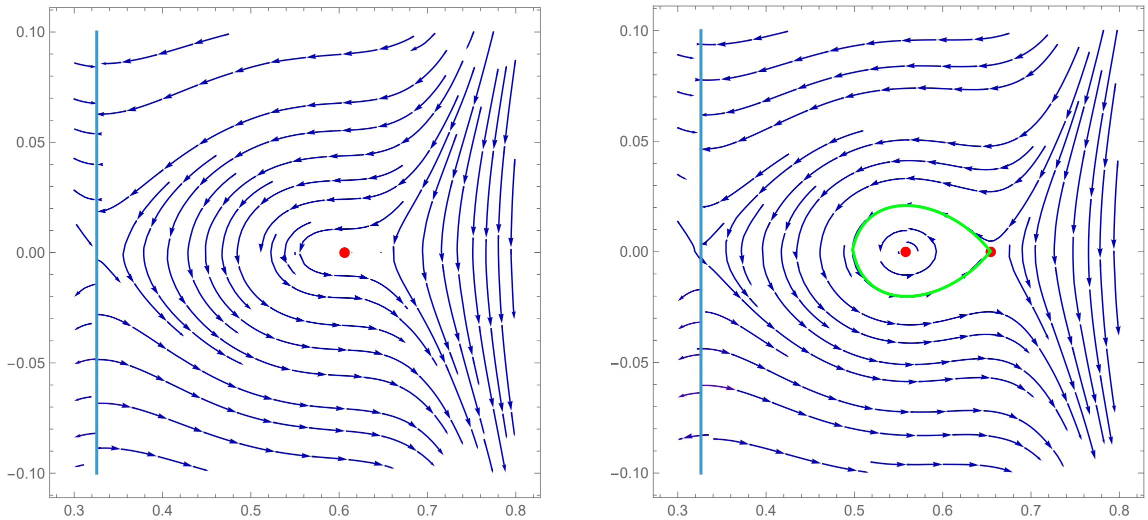

(a) Phase portrait when $\omega = 1$ and $r = 1.1162$. (b) Phase portrait when $\omega = 1$ and $r = 1.118$.

Figure 3.5

increasing $r > r_c$ causes the two equilibrium points to split and one finds two types of solutions. Figure 3.5b shows that the orbit of its limit cycle passes through the second equilibrium point and corresponds to a solitary wave solution, as shown in Figure 3.6a, which illustrates the solution of Figure 3.5b.

As r increases further, the behavior still mirrors that observed in the case of zero vorticity: the limit cycle hits either the equilibrium point or the blue singularity curve, except for some r where it happens at the same time, as illustrated in Figure 3.6b. This limit cycle also corresponds to an extreme solitary wave solution, as shown in Figure 3.3a. The sharp angle at the crest is $\theta = 138.233°$, which, while larger, remains comparable to the classical $120°$ for classical extreme waves in Euler equations.

Further increasing r still shows the same pattern as in the irrotational case, the limit cycle will always intersect the blue singularity curve first. The equilibrium point moves closer to the blue curve as shown in Figure 3.7a. The corresponding solutions are extreme Stokes waves as can be seen in Figure 3.7b, with angle $\theta = 141.548°$ for this solution.

Just as before the equilibrium point becomes unstable once it passes through the blue line; see Figure 3.8a for $r = r_1$. Differences however appear for $r > r_1$ as while the left equilibrium point still moves to the left and the right equilibrium point still moves to the right until it sits on the orange curve, the left point passes zero and passes through the blue singularity curve again as seen in Figure 3.8b. This is still the same curve, although it is not the same point on the curve.

As we increase $r > r_2$ we get similar results to when r was close to r_1, the only differences are that the blue curve is on the right side and there is no second equilibrium point (see Figure 3.9a). The solutions also correspond to extreme Stokes waves which can be seen in Figure 3.9b and has angle $\theta = 51.4732°$ for this solution. Note that this angle is nowhere close to $120°$, indicating a certain difference, compared with the irrotational case.

Increasing r even more causes both the equilibrium point and the blue curve to move left, until the limit cycle intersects the blue curve in two distinct places, as shown in Figure 3.10a.

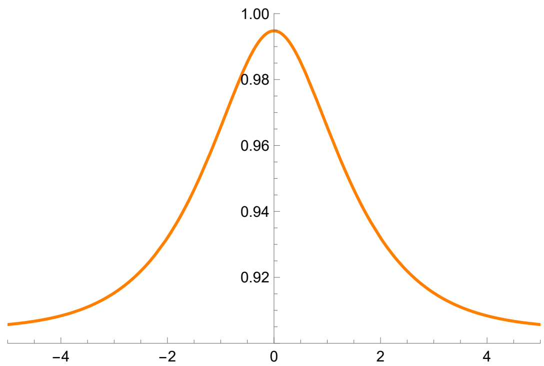

(a) A solution corresponding to the green curve in Figure 3.5b, passing through ($\beta = 0.49645, \alpha = 0$).

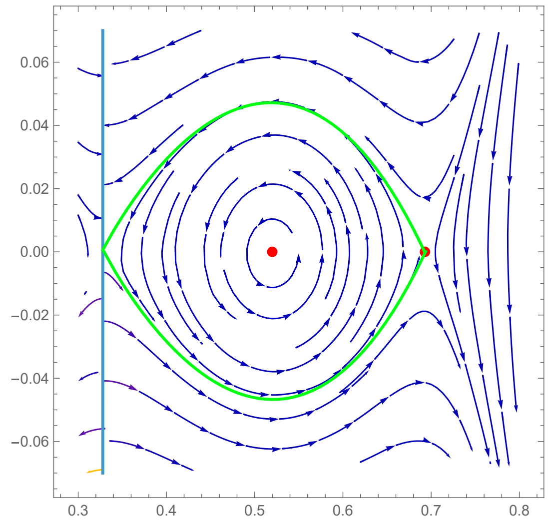

(b) Phase portrait when $\omega = 1$ and $r = 1.122$.

Figure 3.6

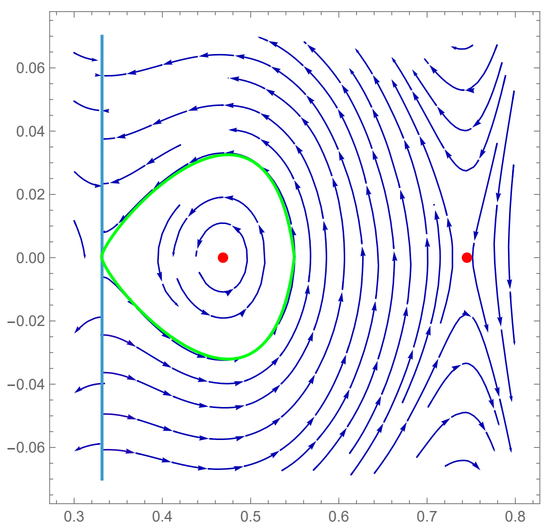

(a) Phase portrait when $\omega = 1$ and $r = 1.131$.

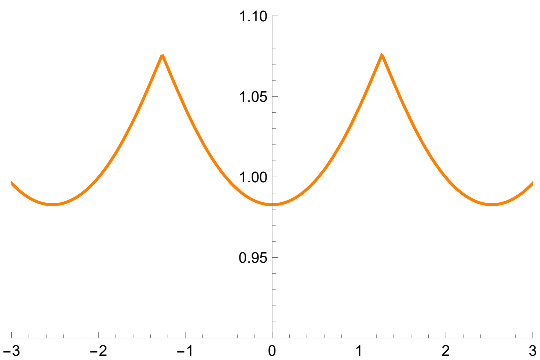

(b) A solution corresponding to the green curve in Figure 3.7a, passing through ($\beta = 0.54449, \alpha = 0$).

Figure 3.7

This corresponds to solutions with two singularities on the side of the wave, where the horizontal velocity attains its maximum along the surface. This somewhat resembles an overhanging wave profile, where horizontal velocity vanishes at some point on the side of the profile. Check Figure 3.10b, which shows the solution of Figure 3.10a.

We note that solutions found for $r > r_2$ correspond to flows with a counter-current. In particular, the horizontal velocity is negative (which coincides with β) at the surface, while it is still positive along the bottom.

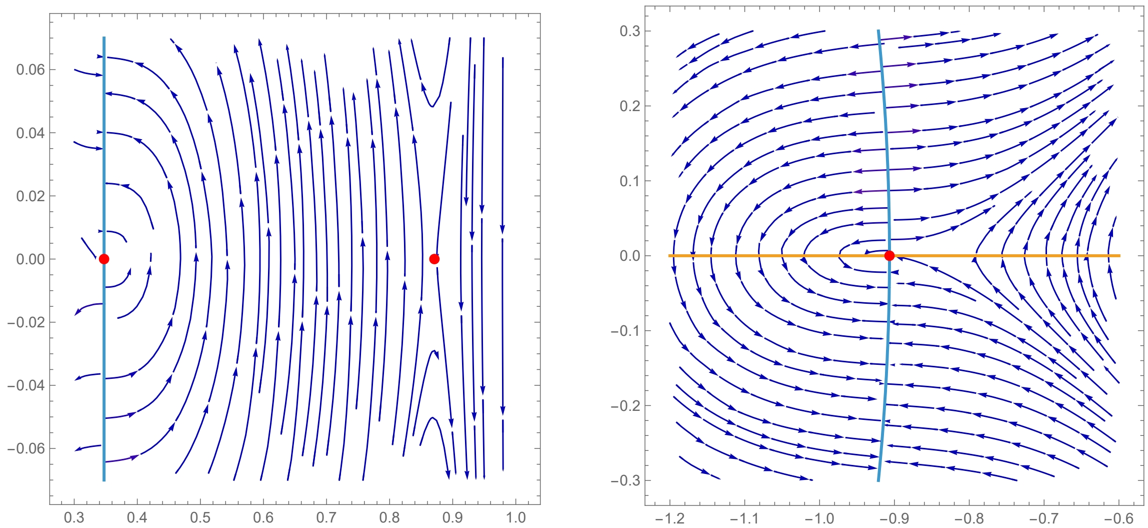

(a) Phase portrait when $\omega = 1$ and $r = 1.16924$.

(b) Phase portrait when $\omega = 1$ and $r = 2.99733$.

Figure 3.8

As ω increases, the structure of the solutions does not change. We have an interval $[r_c\,, r_1]$ where we find, in order, solitary waves, extreme solitary waves and extreme periodic waves as r increases. Then we have a gap where the equilibrium point becomes unstable and lastly we have an interval $[r_2\,, \infty)$, where we find extreme periodic waves and then overhanging waves as r increases.

However, increasing ω causes other changes. In the closed interval, the interval itself shrinks, r_c decreases and the distance between the singularity curve and the second equilibrium point is reduced. Between the intervals, the gap between r_1 and r_2 becomes smaller. In the half open interval, for the phase portrait corresponding to the overhanging solution, the two points at which the limit cycle intersects the singularity curve move closer together—the upper intersection shifts downward and the lower one upward. Furthermore, in both intervals, smaller variations in r are required to change which type of phase portrait is observed, and the limit cycles get relatively flatter, meaning that their vertical-to-horizontal length ratio decreases (at least true for the phase portraits corresponding to extreme solitary waves).

3.1.3 $-0.348705 < \omega < 0$

Next we will analyze the model for $-0.348705 < \omega < 0$, and we will see that it is nearly identical to the case of $\omega > 0$. The only differences are that for r in the second interval $[r_2\,, \infty)$ the equilibrium point moves back to the right past the singularity curve. We also observe some odd behavior when ω approaches -0.348705.

For $-0.348705 < \omega < 0$, when r is in the interval $[r_c\,, r_1]$, we observe identical structure to the case of $\omega > 0$, as illustrated in Figures 3.11, 3.12 and 3.13a. In the gap $r_1 < r < r_2$ the behavior is also similar except for one difference, the equilibrium point will eventually reach a minimum β_{min}, stop moving left and instead move right. Lastly for $r > r_2$, the pattern is

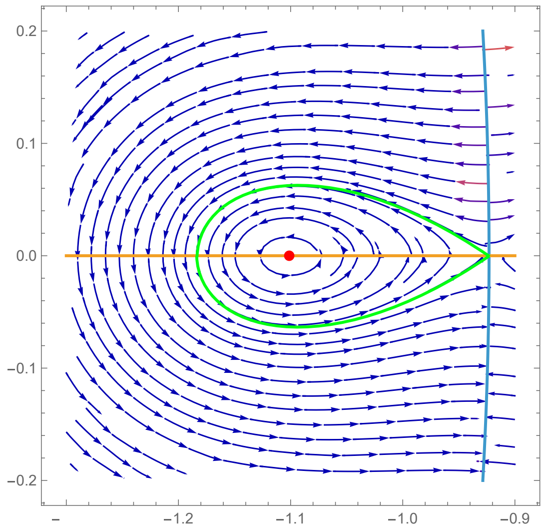

(a) Phase portrait when $\omega = 1$ and $r = 3.5$.

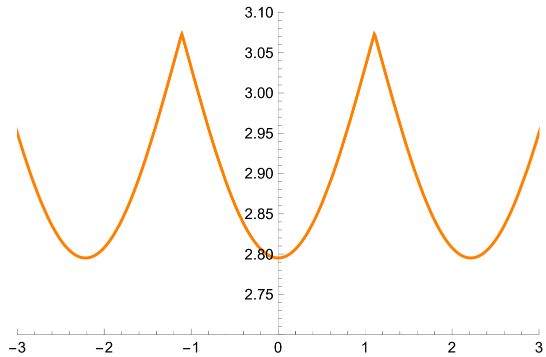

(b) A solution corresponding to the green curve in Figure 3.9a, passing through ($\beta = -1.1873, \alpha = 0$).

Figure 3.9

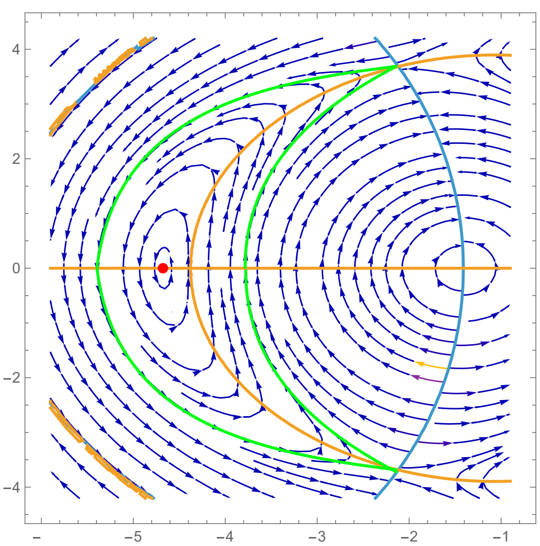

(a) Phase portrait when $\omega = 1$ and $r = 20.5$.

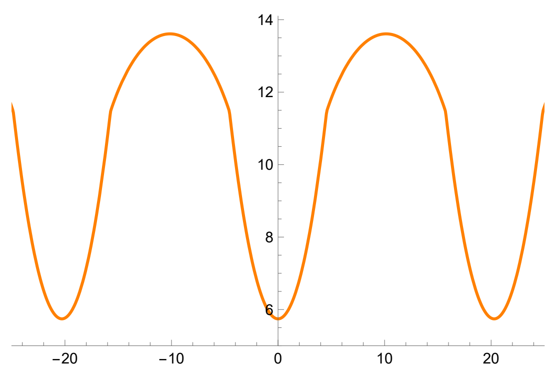

(b) A solution corresponding to the green curve in Figure 3.10a, passing through ($\beta = -5.43273, \alpha = 0$).

Figure 3.10

identical except that the equilibrium point retains a positive value for β and is on the right side of the singularity curve. This can be seen in Figures 3.13b, 3.13c and 3.14.

The solution to Figure 3.12a has angle $\theta = 109.431°$ at the crest, the solution to Figure 3.12b has angle $\theta = 112.04°$ at the crest and the solution to Figure 3.13c has angle $\theta = 106.71°$ at the crest.

As with $\omega > 0$ we note that solutions found for $r > r_2$ correspond to flows with a counter-current. With the difference being that the horizontal velocity is negative at the bottom, while it is still positive along the surface.

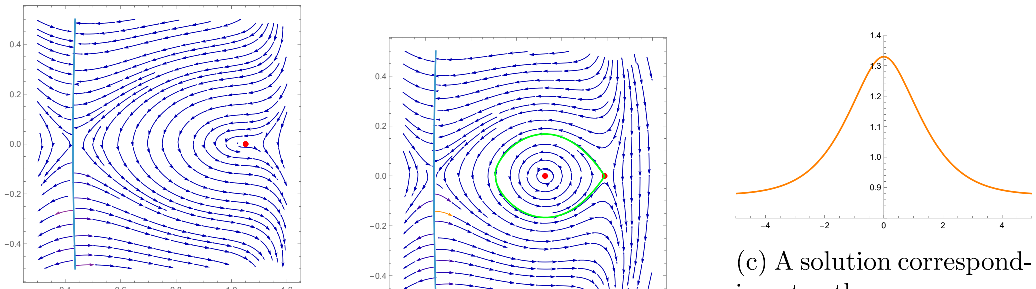

(a) Phase portrait when $\omega = -0.1$ and $r = 1.55125$.

(b) Phase portrait when $\omega = -0.1$ and $r = 1.58$.

(c) A solution corresponding to the green curve in Figure 3.11b, passing through $(\beta = 0.708, \alpha = 0)$.

Figure 3.11

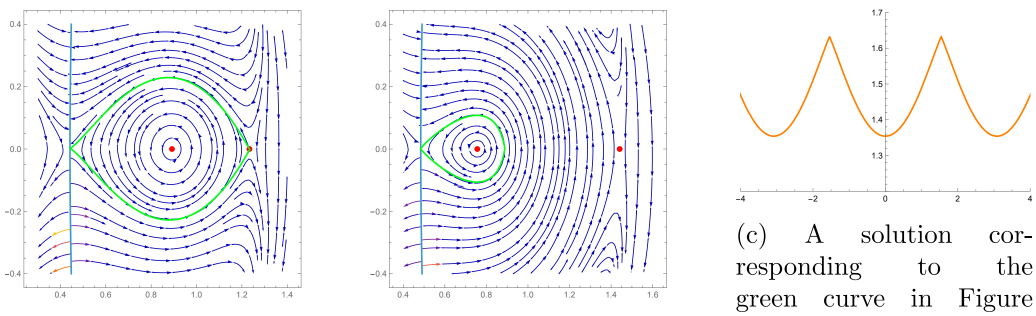

(a) Phase portrait when $\omega = -0.1$ and $r = 1.6$.

(b) Phase portrait when $\omega = -0.1$ and $r = 1.75$.

(c) A solution corresponding to the green curve in Figure 3.12b, passing through $(\beta = 0.88965, \alpha = 0)$.

Figure 3.12

Unlike in the previous case some parts of the structure change as ω decreases. As ω approaches -0.348705 the equilibrium point will hit β_{min} when $r < r_1$, and when $\omega = -0.348705$ there will be no gap between the intervals, meaning $r_1 = r_2$.

Additional we observe other changes ω shrinks, as in the case where $\omega > 0$. In the closed interval, we observe the opposite behavior we saw in the case of positive ω: the size of the closed interval increases and r_c becomes larger. For the open interval, smaller changes in r are required to change which type of phase portrait is observed. Moreover, as in the previous case, for the phase portrait corresponding to the overhanging solution, the two points at which the limit cycle intersects the singularity curve move closer together—the upper intersection shifts downward and the lower one upward. Finally we observe in that, in contrast to the $\omega > 0$ case, the limit cycles get relatively thinner, meaning that their vertical-to-horizontal length ratio increases (at least true for the phase portraits corresponding to extreme solitary waves).

3.1.4 $\omega < -0.34870$

Lastly we analyze the model for $\omega < -0.348705$, which structure changes greatly as ω decreases. Notably we find less and less unique solutions.

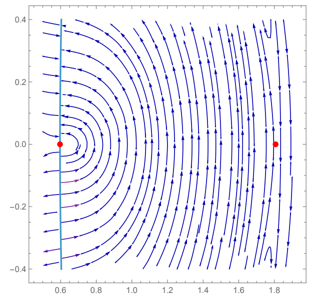

(a) Phase portrait when $\omega = -0.1$ and $r = 2.19444$.

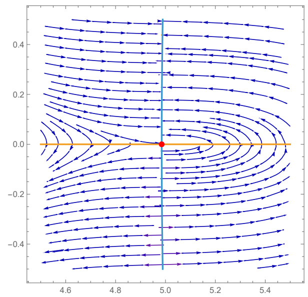

(b) Phase portrait when $\omega = -0.1$ and $r = 111.921$.

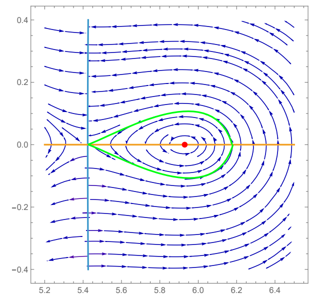

(c) Phase portrait when $\omega = -0.1$ and $r = 136.0$.

Figure 3.13

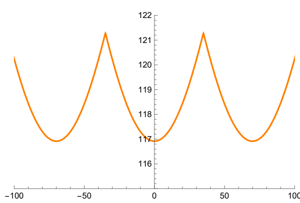

(a) A solution corresponding to the green curve in Figure 3.13c, passing through $(\beta = 6.17797, \alpha = 0)$.

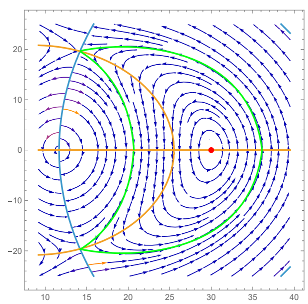

(b) Phase portrait when $\omega = -0.1$ and $r = 1050.0$.

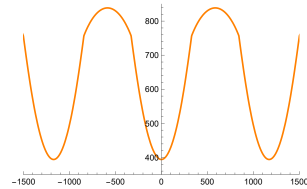

(c) A solution corresponding to the green curve in Figure 3.14b, passing through $(\beta = 36.21717, \alpha = 0)$.

Figure 3.14

For $\omega < -0.348705$, there is no longer two intervals and as such we find solutions for r in the interval $[r_c\,, \infty)$.

When ω is close to -0.348705 we still have the same structure as for $-0.348705 < \omega < 0$ except that the equilibrium point never passes through the singularity curve and thus we have only one interval. This is illustrated in Figure 3.15, 3.16, 3.17 and 3.18.

The solution to Figure 3.16a has angle $\theta = 105.309°$ at the crest, the solution to Figure 3.16b has angle $\theta = 102.38°$ at the crest and the solution to Figure 3.17a has angle $\theta = 97.3579°$ at the crest.

As ω decreases the structure of solutions changes greatly, first we lose the extreme periodic wave solutions, then the extreme solitary wave solution, until we only have solitary wave solutions and overhanging wave solutions; see Figure 3.19 and 3.20. We do hoverer gain a new solution, solitary overhanging waves as seen in Figure 3.21, and a sketch of the corresponding solution is shown in Figure 3.21b.

As can be seen clearly in Figure 3.22b, the phase portrait is already evolving toward the structure characteristic of an overhanging wave: see Figure 3.23a. This means we do no get an extreme solitary wave solution.

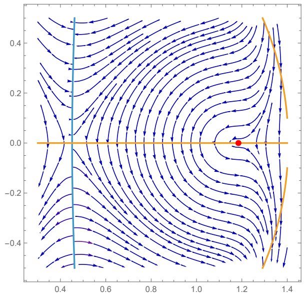

(a) Phase portrait when $\omega = -0.353$ and $r = 1.69192$.

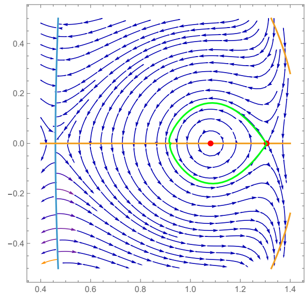

(b) Phase portrait when $\omega = -0.353$ and $r = 1.72$.

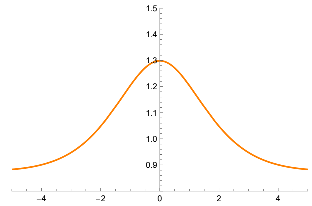

(c) A solution corresponding to the green curve in Figure 3.15b, passing through $(\beta = 0.918, \alpha = 0)$.

Figure 3.15

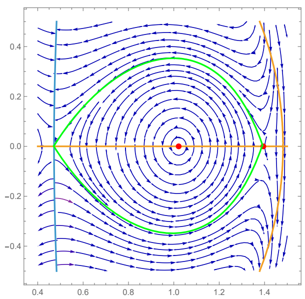

(a) Phase portrait when $\omega = -0.353$ and $r = 1.77$.

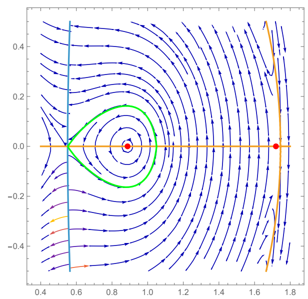

(b) Phase portrait when $\omega = -0.353$ and $r = 2.1$.

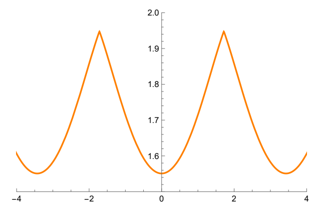

(c) A solution corresponding to the green curve in Figure 3.16b, passing through $(\beta = 1.04792, \alpha = 0)$.

Figure 3.16

As ω decreases smaller changes in r are required to change which type of phase portrait is observed (seemingly, but hard to tell), r_c is larger and the curve tips touching the walls in stage 8 are closer (higher one is lower down and lower one is higher up).

Furthermore, As ω decreases r_c becomes larger. It also seems smaller changes in r are required to change which type of phase portrait is observed and the two points at which the limit cycle intersects the singularity curve move closer together—the upper intersection shifts downward and the lower one upward. This is difficult to tell as unique solutions disappear and fuse.

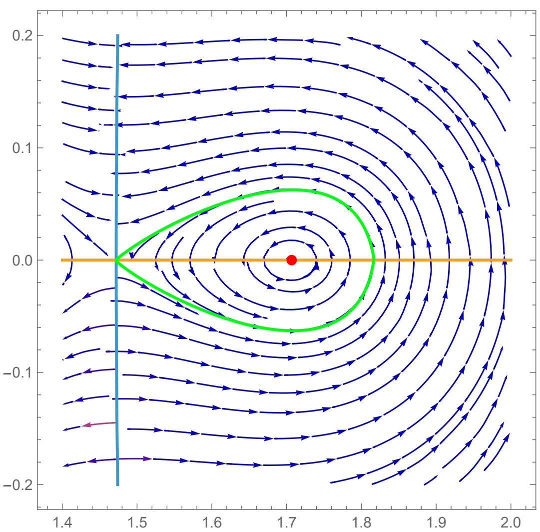

(a) Phase portrait when $\omega = -0.353$ and $r = 10.5$.

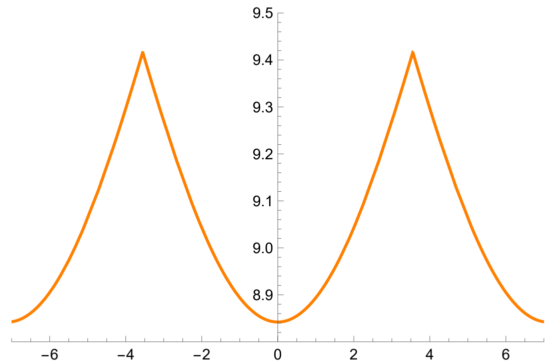

(b) A solution corresponding to the green curve in Figure 3.17a, passing through ($\beta = 1.8209518, \alpha = 0$).

Figure 3.17

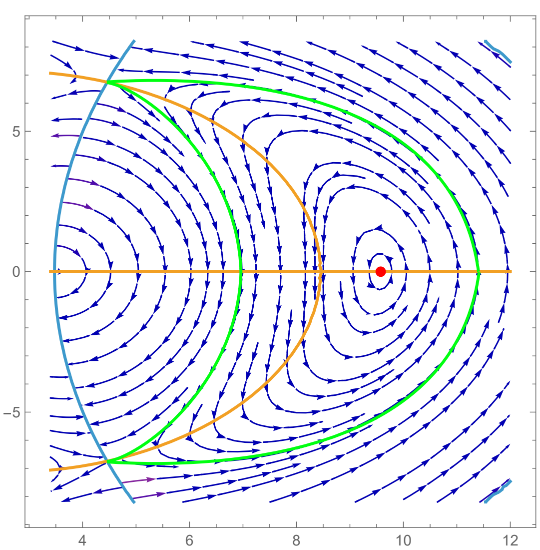

(a) Phase portrait when $\omega = -0.353$ and $r = 100.0$.

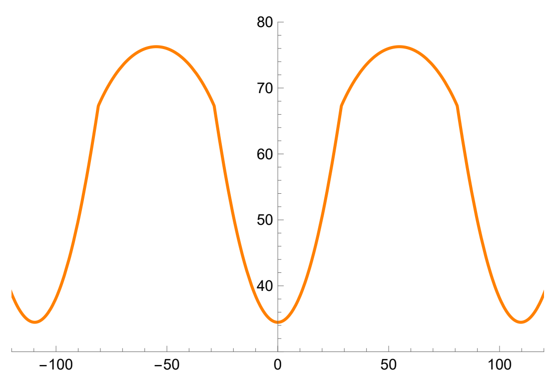

(b) A solution corresponding to the green curve in Figure 3.18a, passing through ($\beta = 11.448276, \alpha = 0$).

Figure 3.18

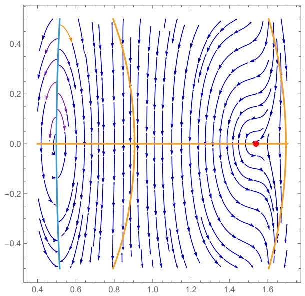

(a) Phase portrait when $\omega = -1$ and $r = 2.1162$.

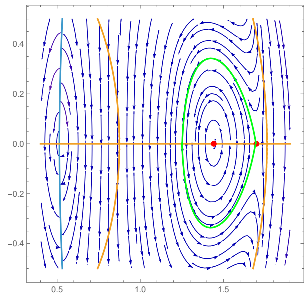

(b) Phase portrait when $\omega = -1$ and $r = 2.2$.

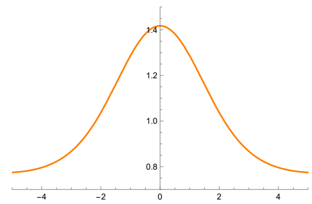

(c) A solution corresponding to the green curve in Figure 3.19b, passing through $(\beta = 1.251, \alpha = 0)$.

Figure 3.19

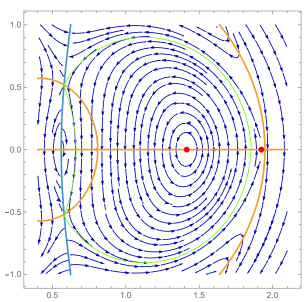

(a) Phase portrait when $\omega = -1$ and $r = 2.47$.

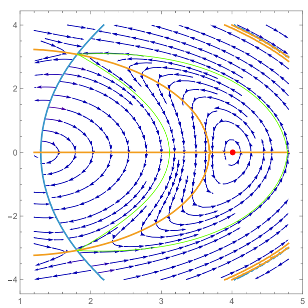

(b) Phase portrait when $\omega = -1$ and $r = 15.8$.

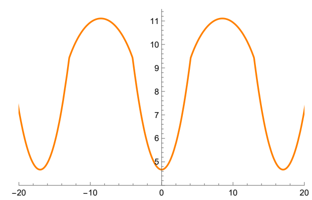

(c) A solution corresponding to the green curve in Figure 3.20b, passing through $(\beta = 4.718105, \alpha = 0)$.

Figure 3.20

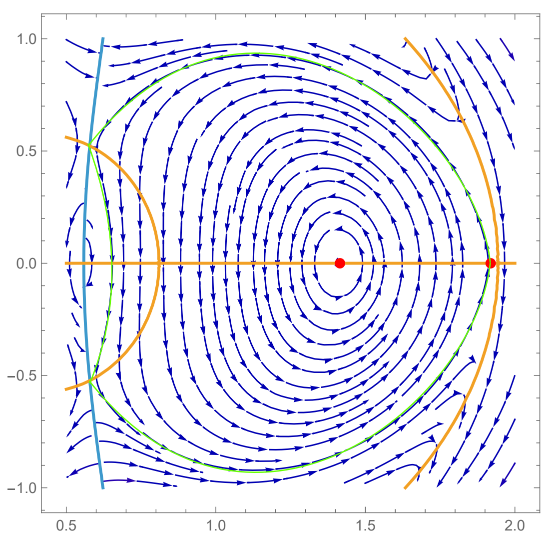

(a) Phase portrait when $\omega = -1$ and $r = 2.463$.

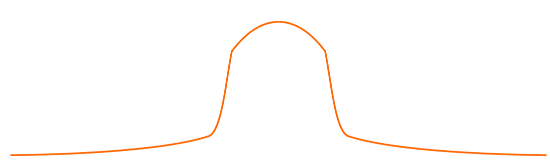

(b) A sketch of the solution corresponding to the green curve in Figure 3.21a.

Figure 3.21

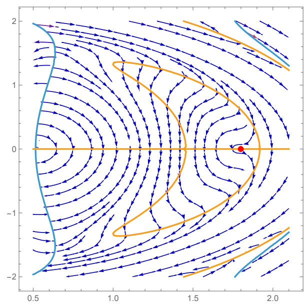

(a) Phase portrait when $\omega = -1.5$ and $r = 2.49339$.

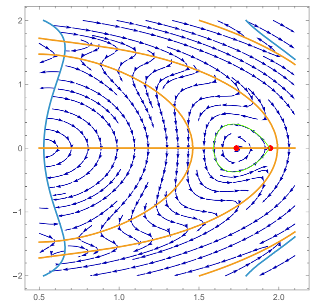

(b) Phase portrait when $\omega = -1.5$ and $r = 2.6$.

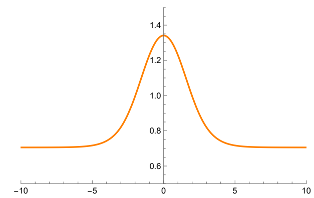

(c) A solution corresponding to the green curve in Figure 3.22b, passing through $(\beta = 1.5867778, \alpha = 0)$.

Figure 3.22

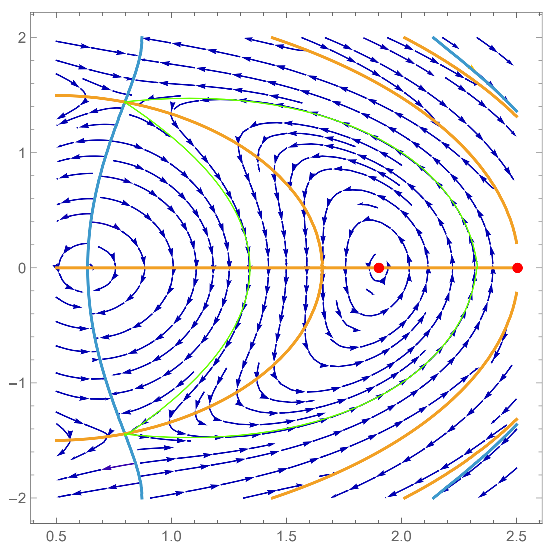

(a) Phase portrait when $\omega = -1.5$ and $r = 3.6$.

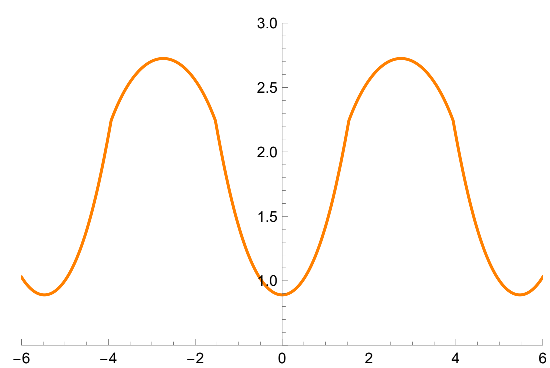

(b) A solution corresponding to the green curve in Figure 3.23a, passing through $(\beta = 2.327911, \alpha = 0)$.

Figure 3.23

Bibliography

[1] C. J. Amick, L. E. Fraenkel, and J. F. Toland, *On the stokes conjecture for the wave of extreme form*, Acta Mathematica **148** (1982), no. none, 193 –214.

[2] Adrian Constantin, *Nonlinear water waves with applications to wave-current interactions and tsunamis*, Society for Industrial and Applied Mathematics, 2011.

[3] Susanna V. Haziot, Vera Mikyoung Hur, Walter Strauss, J. F. Toland, Erik Wahlén, Samuel Walsh, and Miles H. Wheeler, *Traveling water waves – the ebb and flow of two centuries*, 2021.

[4] Tatsuo Iguchi, *Isobe–kakinuma model for water waves as a higher order shallow water approximation*, Journal of Differential Equations **265** (2018), no. 3, 935–962.

[5] M. A. Lavrentiev, *On the theory of long waves. II. a contribution to the theory of long waves*, American Mathematical Society Translations **102** (1954), 53. MR0061952

[6] A. I. Nekrasov, *On steady waves*, Izvestiya Ivanovo-Voznesensk Polytechnic Institute **In-ta 3** (1921).

[7] G. G. Stokes, *Considerations relative to the greatest height of oscillatory irrotational waves which can be propagated without change of form*, Mathematical and Physical Papers **1** (1880), 225–228.

[8] J. F. Toland, *Stokes waves*, Topological Methods in Nonlinear Analysis **7** (1996), no. 1, 1 –48.